

Model atmospheres of chemically peculiar stars

Self-consistent empirical stratified model of HD 24712

D. Shulyak¹, T. Ryabchikova^{1,2}, L. Mashonkina², and O. Kochukhov³

¹ Institute of Astronomy, Vienna University, Turkenschanzstrasse 17, 1180 Vienna, Austria

² Institute of Astronomy, Russian Academy of Science, Pyatnitskaya 48, 119017 Moscow, Russia

³ Department of Astronomy and Space Physics, Uppsala University, Box 515, 751 20, Uppsala, Sweden

Received / Accepted

ABSTRACT

Context. High-resolution spectra of some chemically peculiar stars clearly demonstrate the presence of strong abundance gradients in their atmospheres. However, these inhomogeneities are usually ignored in the standard scheme of model atmosphere calculations, braking the consistency between model structure and spectroscopically derived abundance pattern.

Aims. In this paper we present first empirical self-consistent stellar atmosphere model of roAp star HD 24712 with stratification of chemical elements included, and which is derived directly from the observed profiles of spectral lines without time-consuming simulations of physical mechanisms responsible for these anomalies.

Methods. We used the LLMODELS stellar model atmosphere code and DDAFIT minimization tool for analysis of chemical elements stratification and construction of self-consistent atmospheric model. Empirical determination of Pr and Nd stratification in the atmosphere of HD 24712 is based on NLTE line formation for Pr II/III and Nd II/III with the use of the DETAIL code.

Results. Based on iterative procedure of stratification analysis and subsequent re-calculation of model atmosphere structure we constructed a self-consistent model of HD 24712, i.e. the model which temperature-pressure structure is consistent with results of stratification analysis. It is shown that stratification of chemical elements leads to the considerable changes in model structure as to compare with non-stratified homogeneous case. We find that accumulation of REE elements allows for the inverse temperature gradient to be present in upper atmosphere of the star with the maximum temperature increase of about 600 K.

Conclusions.

Key words. stars: chemically peculiar – stars: atmospheres – stars: individual: HD 24712

1. Introduction

Atmospheres of chemically peculiar (CP) stars exhibit the presence of inhomogeneous distribution of chemical elements. These inhomogeneities are frequently seen as abundance spots on stellar surfaces (see, for example, Kochukhov et al. 2004a,b; Lueftinger et al. 2003) and as clouds of chemical elements concentrated at certain depths along the stellar radii (Ryabchikova et al. 2006, 2005, 2002). Several tools have been developed and successfully applied to the analysis of element distributions based on detailed analysis of observed line profiles. The horizontal elements distribution is investigated using the rotational modulation of spectral lines: as star rotates, the abundance spots on its surface should reveal themselves as variation of line profiles of respective elements observed at different rotational phases of the star. The automatic procedure of finding the spots position and abundance values via the comparison of observed and calculated spectra is performed via Doppler Imaging techniques firstly introduced by Goncharsky et al. (1982) and further developed by Piskunov & Wehlau (1990) (see also Kochukhov et al. (2004b)). The vertical distribution of chemical elements is modeled assuming the stratification profiles of chemical elements to be represented by simple step-function with two different abundances in upper and lower atmosphere as was suggested in Babel

(1992), or, as recently showed by Kochukhov et al. (2006), applying the regularized minimization algorithm. The results of these analyses show that strong abundance gradients do exist in atmospheres of CP stars with accumulation of various chemical elements at different atmospheric layers.

From theoretical point of view, the appearance of inhomogeneous element distribution with high abundance gradients in atmospheres of CP stars is explained by microscopic radiative diffusion processes: the atmospheres of these stars are believed to be dynamically stable enough for radiative levitation and gravitational settling to rule the distribution of chemical elements (Michaud 1970).

These abundance inhomogeneities may have rather strong influence on model atmosphere structure via modification of opacity and emissivity coefficients and thus the modeling of element distributions in stellar atmospheres should, in principle, include the simulation of these diffusion processes on every step of model atmosphere calculation. Such models were successfully developed and improved in last years (see, for example, Hui-Bon-Hoa et al. 2000; Alecian & Stift 2007), however, the sensitivity of modeled element distributions to the input physics (that is frequently poorly understood), the absence of accurate atomic data for some elements, and high computational expenses do not allow implementation of these models for detailed modeling of theoretical line profiles and their comparison with high-resolution observations: although the theoretical stratification is able to predict some observed characteristics of CP stars, it is

still not applied for the quantitative interpretations of modern high-resolution spectroscopic observations.

One of the necessary ingredient in analysis of elements stratification is the computation of synthetic spectra and their subsequent comparison with observations: a set of such computations is needed to construct the stratification profile of a given element that ensures a best fit between theoretical and observed line profiles. These empirical investigations of elements stratification in stellar atmospheres are very important for understanding the physical conditions in atmospheres of CP stars and, ideally, should provide the test ground for recent theoretical calculations. The only methodological difficulty in empirical analysis is that almost in all cases the synthetic spectrum is computed using standard model atmospheres, i.e. model atmosphere that were computed under the assumption of homogeneous elements distribution.

To avoid this inconsistency we made an attempt to implement an iterative procedure of vertical stratification analysis with the subsequent re-calculation of model atmosphere structure. This procedure is applied to cool roAp star HD 24712 for which the stratification of Si, Ca, Cr, Fe, Sr, Ba, Pr, and Nd is derived. Stratification analysis of Pr and Nd is based on non-local thermodynamic equilibrium (NLTE) line formation for Pr II/III and Nd II/III. Using this approach we examine how the stratification profiles of different elements are changing comparing with the case when only non-stratified model is applied and what is the overall effect of inhomogeneous elements distribution on model atmosphere structure.

In the next section we give an overview of observations used. Then, in Sect. 3 we describe the general methods and atomic line data used for analysis of element stratification. In Sect. 4 we present the results of stratification analysis and its effect on model atmosphere structure and some observed parameters of the star. The main conclusions are summarized in Sect. 5

2. Observations

We used an average spectrum of HD 24712 obtained at November 10/11, 2004, with HARPS (High Accuracy Radial velocity Planet Searcher) spectrometer at the 3.6-m telescope at ESO, La Silla. The details of the reduction procedure are given in Ryabchikova et al. (2007). In total 92 spectra were taken with 60 s exposure time, signal to noise ratio $S/N = 120$, and $R = 120\,000$ resolving power. These spectra cover a spectral region from 3850\AA to 6730\AA . After averaging the final $S/N = 1000$ was reached. HARPS spectra were obtained at the phase 0.867 close to magnetic maximum (Ryabchikova et al. 2007). Photometric color-indices were taken from the SIMBAD electronic database¹ with the additional Strömgren photometry from Martinez (1993), peculiar index a from Vogt et al. (1998), and Geneva colors from Burki et al. (1999). We also used UV spectroscopic observations extracted from IUE data archive².

3. Methods

3.1. Stratification analysis

To analyse the stratification of chemical elements in the atmosphere of HD 24712 we applied step-function approximation as performed in DDAFIT – an automatic procedure for determination of vertical abundance gradients (Kochukhov 2007) that was

successfully used in a number of studies (e.g. Ryabchikova et al. 2006, 2005, 2008). In this routine, the vertical abundance distribution of an element is described by four parameters: chemical abundance in the upper atmosphere, abundance in deep layers, the position of the abundance jump and the width of the transition region where chemical abundance changes between the two values. All four parameters can be optimized simultaneously with the least-squares fitting procedure and based on observations of unlimited number of spectral regions. DDAFIT also allows the stratification analysis with the magnetically-split lines. For HD 24712 we assumed a pure radial magnetic field with the modulus $\langle B \rangle = 3.1$ kG (Ryabchikova et al. 2007). The spectral synthesis was performed using SYNTHMAG code (Kochukhov 2007) which represents an improved version of the program developed by Piskunov (1999).

For Pr and Nd, we performed NLTE stratification analysis as described in Mashonkina et al. (2009) and Mashonkina et al. (2005) using a trial-and-error method and the observed equivalent widths of the lines of the first and second ions.

3.2. NLTE calculations

The present investigation of Pr II/III and Nd II/III is based on the NLTE methods treated in our earlier studies (Mashonkina et al. 2009) and (Mashonkina et al. 2005), where atomic data and the problems of line formation have been considered in detail. To describe briefly, comprehensive model atoms of praseodymium and neodymium include the measured and the predicted energy levels, in total, 6708 levels of Pr II and Pr III and 2258 levels of Nd II and Nd III. The coupled radiative transfer and statistical equilibrium equations were solved using a revised version of the DETAIL program (Butler & Giddings 1985) based on the accelerated lambda iteration, which follows the efficient method described by Rybicki & Hummer (1991, 1992).

As shown for Nd by Mashonkina et al. (2005) and for Pr by Mashonkina et al. (2009), the main non-LTE effect for their first ions in the model atmosphere representing the atmosphere of HD 24712, is overionization caused by a super-thermal radiation of non-local origin close to the thresholds of the low-excitation levels. The departures from LTE for the lines of the first and the second ions are of the opposite sign and they are significant if the element is concentrated in the uppermost atmospheric layers where collisions are inefficient in establishing thermodynamic equilibrium. For the Pr and Nd distribution in the atmosphere of HD 24712 determined by Mashonkina et al. (2009) and Mashonkina et al. (2005), the NLTE abundance corrections, $\Delta\epsilon_{\text{NLTE}} = \epsilon_{\text{NLTE}} - \epsilon_{\text{LTE}}$, are positive for the lines of Pr II and Nd II and constitute between 1.0 dex and 1.4 dex, while $\Delta\epsilon_{\text{NLTE}}$ is negative for the lines of Pr III and Nd III and ranges between -0.3 dex and -0.7 dex.

We performed NLTE calculations for H I using the method described in Mashonkina et al. (2008). The model atom includes levels with principal quantum numbers up to $n = 19$. For the model atmospheres investigated in this study, the ground state keeps their thermodynamic equilibrium level populations throughout the atmosphere. In the layers where the core-to-wing transition is formed, namely, between $\log \tau_{5000} \approx -1.2$ and $\log \tau_{5000} \approx -2.2$, the $n = 2$ level is closely coupled to the ground state, while departures from LTE for the $n = 3$ level are controlled by H α which serves as the pumping transition resulting in an overpopulation of the upper level. For H α , NLTE leads to weakening of the core-to-wing transition compared to the LTE case.

¹ <http://simbad.u-strasbg.fr/simbad/>

² <http://ines.ts.astro.it/>

3.3. Model atmospheres

To perform the model atmosphere calculations we used the recent version of the LLMODELS (Shulyak et al. 2004) stellar model atmosphere code (version 8.6). LLMODELS is 1-D, hydrostatic, plain-parallel LTE code which accounts for the effects of individual and stratified abundances. It is to note that the stratification of chemical elements is an input parameter for LLMODELS code and thus is not changing during model atmosphere calculation process. This allows to explore the changes in model structure due to stratification that was extracted directly from observations without modeling the processes that could be responsible for the observed inhomogeneities.

The following calculation settings were used for every model atmosphere calculation: the atmosphere of a star is discretized into 120 layers between $\log \tau_{5000} = -8$ and 2 with a non-equidistant spacing, i.e. with the higher points density in the regions of steep abundance gradients to ensure accurate integration of radiation field properties and solution of other model equations. The frequency-dependent quantities are calculated with variable wavelength step: 0.1 between 500Å and 20 000Å, and 0.5Å between 20 000Å and 70 000Å respectively. VALD database (Piskunov et al. 1995; Kupka et al. 1999) was used as a source of atomic lines data for computation of line absorption coefficient.

The use of the LTE assumption in atmosphere modeling results from the following consideration. The opacity in the atmosphere of HD 24712 is mostly contributed by neutral hydrogen. Our NLTE calculations for H I showed no significant deviations from thermodynamic equilibrium populations for the $n = 1$ level throughout the atmosphere and for the $n = 2$ level below $\log \tau_{5000} = -3$. The departures from LTE are found to be larger for the hotter atmosphere of Vega, however, self-consistent NLTE modelling of Hauschildt et al. (1999) leads to only 200–300 K changes in T distribution compared to the LTE model in the layers between $\log \tau_{5000} = -1$ and $\log \tau_{5000} = -6$. The NLTE effect on atmospheric structure of HD 24712 is expected to be smaller. Another important opacity contributors are the iron group elements. The iron and chromium among them are concentrated in deep atmospheric layers of HD 24712, below $\log \tau_{5000} = -2$ (see Fig. 3), where the departures from LTE are expected to be small. This is confirmed by our NLTE calculations for Ca which distribution in the atmosphere is similar to that for the iron group elements (Fig. 3). We used the NLTE method for Ca I/II described by Mashonkina et al. (2007). We do not know the distribution of light elements, C, N, and O, however, according to Khan & Shulyak (2006) these elements do not introduce noticeable changes in model structure and emergent flux. The influence of the departures from LTE for two rare-earth elements (REE), Pr and Nd, on atmospheric structure of HD 24712 is simulated in present paper.

Finally, the magnetic field with the intensity less than 5 kG has marginal impact on model temperature-pressure structure (Kochukhov et al. 2005; Khan & Shulyak 2006). Thus, we ignored the effects of polarized radiative transfer and Zeeman splitting in all model atmosphere calculations presented in this study.

3.4. Atomic line data for stratification analysis

As was emphasized in Ryabchikova et al. (2003) the vertical abundance stratification manifests itself as an impossibility to fit the core and wings of strong lines with developed Stark wings (Ca II K, Si II, Mg II lines, etc.) with the same abundance or as

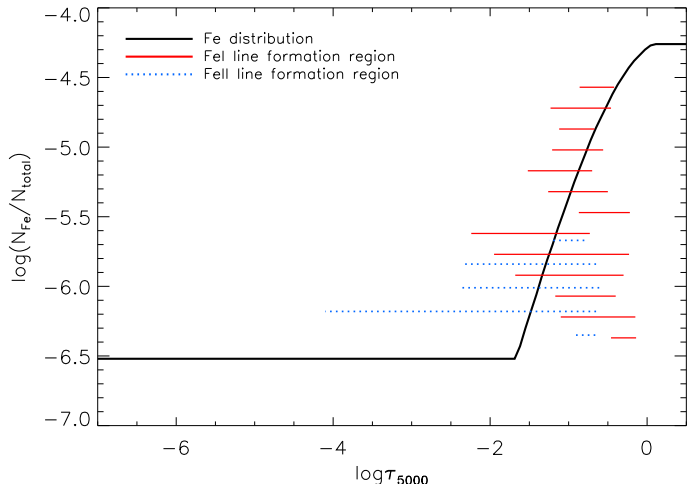


Fig. 1. Fe abundance distribution derived with the homogeneous model atmosphere and the range of the optical depth formation of Fe I and Fe II lines from Table 1 calculated with homogeneous Fe abundance $\log(Fe/N_{\text{total}}) = -5.10$.

an impossibility to describe the low and high-excitation lines of the same ion with a chemically homogeneous atmosphere. It means that the choice of a proper set of spectral lines is crucial for element stratification study. Ideally, it should be a set of lines originated from the levels in large range of the excitation energies and from different ions, thus probing a substantial part of stellar atmosphere. In chemically peculiar stars as cool as HD 24712 we deal with severe blending by numerous lines of the rare-earth elements, therefore the strongest lines with the developed wings (like, for example, Fe I $\lambda 4045.8$ Å line) are not possible to use. Also, Fe II lines with the upper level excitation potential at 10 eV and higher are not visible any longer. The blue spectral region is more crowded with the REE lines than the red one and the preferential working spectral region is 5000–6800Å. Table 1 gives a list of Si, Ca, Cr, Fe, Sr, Ba lines used in LTE stratification analysis routines together with the atomic parameters and the references. For NLTE stratification analysis we used the same lines as given in the papers of Mashonkina et al. (2005) and Mashonkina et al. (2009).

An ability of the chosen set of spectral lines to probe different atmospheric layers is illustrated in Fig. 1. The iron stratification derived with the initial model (see Section 4) is shown together with the ranges of Fe lines depth formation calculated on $\log \tau_{5000}$ scale. The later were calculated with the contribution function to the emergent line radiation following Achmad et al. (1991). Fig. 2 illustrates a fit of the calculated to the observed Fe line profiles for homogeneous and stratified atmospheres. For Si, Ca, Cr, Sr, and Ba the corresponding plots are shown in Figs. 7,8,9,10 (Online material).

3.5. Self-consistent models with empirical stratification

Using the methods of stratification analysis described above one could restore the element distribution profile of any chemical elements for which accurate atomic line data exist. However, we should remember that the empirical analysis of chemical elements stratification is based on model atmosphere technique, and thus the temperature-pressure structure of model atmosphere itself depends upon stratification which has to be found. Therefore, the calculation of model atmosphere and stratification (abundances) analysis are linked together and thus an iterative

Table 1. A list of spectral lines used for the stratification calculations. The columns give the ion identification, central wavelength, the excitation potential (in eV) of the lower level, oscillator strength ($\log(gf)$), the Stark damping constant (“appr” marks lines for which the classical approximation was used), and the reference for oscillator strength.

Ion	Wavelength	E_i (eV)	$\log(gf)$	$\log \gamma_{St}$	Ref.	Ion	Wavelength	E_i (eV)	$\log(gf)$	$\log \gamma_{St}$	Ref.
Si II	5056.320	10.074	-0.510	-4.78	BBC	Cr II	6147.154	4.756	-2.89	-6.66	RU
Si I	5517.530	5.082	-2.490	appr	astr	Fe II	5132.669	2.807	-4.09	-6.600	RU
Si I	5780.380	4.920	-2.350	-4.18	G	Fe II	5169.033	2.891	-1.25	-6.590	RU
Si I	5948.540	4.930	-1.230	-4.27	G	Fe II	5197.480	5.960	-3.13	-6.700	RU
Si II	5978.930	10.074	-0.030	-5.01	BBC	Fe II	5197.577	3.230	-2.10	-6.600	RU
Si I	6142.480	5.619	-1.420	appr	astr	Fe I	5198.711	2.223	-2.135	-6.190	MFW
Si I	6155.130	5.619	-0.800	appr	astr	Fe I	5217.389	3.211	-1.070	-5.450	BKK
Si II	6347.110	8.121	0.230	-5.31	BBC	Fe I	5253.462	3.283	-1.44	-5.460	K07
Si II	6371.350	8.121	-0.080	-5.32	BBC	Fe I	5383.369	4.312	0.645	-5.180	BWL
Ca I	4226.728	0.000	0.244	-6.03	SG	Fe I	5397.127	0.915	-1.993	-6.300	MFW
Ca II	5021.138	7.515	-1.207	-4.61	TB	Fe I	5397.190	4.446	-1.16	-5.260	K07
Ca II	5285.138	7.515	-1.207	-4.61	TB	Fe I	5410.910	4.470	0.398	-5.060	BWL
Ca I	5857.451	2.933	0.240	-5.42	S	Fe I	5424.068	4.320	0.520	-4.790	MFW
Ca I	5867.562	2.933	-1.570	-4.70	S	Fe II	5425.257	3.199	-3.16	-6.600	RU
Ca I	6162.173	1.899	-0.090	-5.32	SO	Fe I	5434.523	1.011	-2.122	-6.303	BPS1
Ca I	6163.755	2.521	-1.286	-5.00	SR	Fe I	5560.211	4.434	-1.05	-4.323	K07
Ca I	6169.042	2.253	-0.797	-5.00	SR	Fe I	5576.089	3.430	-1.000	-5.490	MFW
Ca I	6455.598	2.523	-1.340	-6.07	S	Fe I	5775.081	4.220	-1.15	-5.560	K07
Ca II	6456.875	8.438	0.410	-3.70	TB	Fe I	6137.691	2.588	-1.403	-6.112	BPS2
Ca I	6471.662	2.526	-0.686	-6.07	SR	Fe I	6336.824	3.686	-0.856	-5.467	BK
Cr I	4274.800	0.000	-0.231	-6.22	MFW	Fe II	6432.680	2.891	-3.52	-6.690	RU
Cr II	4592.050	4.074	-1.419	-6.65	NL	Sr II	4161.792	2.940	-0.502	appr	W
Cr II	4634.070	4.072	-0.980	-6.65	NL	Sr II	4215.519	0.000	-0.145	-5.50*	W
Cr II	5046.429	8.227	-1.75	-5.91	RU	Sr I	4811.877	1.847	0.190	appr	GC
Cr II	5267.030	4.042	-3.06	-6.72	RU	Sr I	5504.177	2.259	0.090	appr	GC
Cr I	5296.691	0.983	-1.400	-6.12	MFW	Sr I	6408.459	2.271	0.510	appr	GC
Cr I	5297.377	2.900	0.167	-4.31	MFW	Ba II	4166.000	2.722	-0.42	appr	NBS
Cr I	5348.315	1.004	-1.290	-6.11	MFW	Ba II	4524.925	2.512	-0.36	appr	NBS
Cr II	5510.700	3.827	-2.610	-6.65	RU	Ba II	4554.029	0.000	0.17	appr	NBS
Cr II	5569.110	10.872	0.860	-5.36	RU	Ba II	5853.668	0.604	-1.00	appr	NBS
Cr II	6053.466	4.745	-2.230	-6.63	RU	Ba II	6141.713	0.704	-0.076	appr	NBS
Cr II	6070.100	4.750	-2.990	-6.63	RU	Ba II	6496.897	0.604	-0.377	appr	NBS
Cr II	6138.721	6.484	-2.160	-6.73	RU						

G – Garz (1973); BBC – Blanco et al. (1995); SG – Smith & Gallagher (1966); SMP – Seaton et al. (1994); S – Smith (1988); SO – Smith & O’Neil (1975); SR – Smith & Raggett (1981); RU – Raassen & Uylings (1998); MWF – Martin et al. (1988); NL – Nilsson et al. (2006); BWL – Black et al. (1972); BPS1 – Blackwell et al. (1979); BPS2 – Blackwell et al. (1982); BK – Bard & Kock (1994); BKK – Bard et al. (1994); K07 – Kurucz database³) W – Warner (1968); GC – Garcia & Campos (1988); * – Fleurier et al. (1977); NBS – Miles & Wiese (1969).

procedure should be used in this case. In general, this procedure could be divided into several steps:

1. calculation of so-called first approximation, simplified model, that could be any standard model atmosphere with the atmospheric parameters close to those of the star to be analysed;
2. determination of stratification of chemical elements based on spectroscopic analysis of individual spectral lines;
3. calculation of improved model atmosphere taking into account stratification found in previous step;
4. comparison of modeled energy distribution (or/and photometric colors) and hydrogen line profiles with observed ones and re-adjustments of model input parameters (T_{eff} , $\log g$) if needed to fit observations. At this step several calculations of model atmosphere with fixed stratification but different model parameters may be required;
5. repeating the overall process starting from step 2 until stratification profiles of chemical elements and model parameters are not converged.

At the end, the listed above procedure ensures the consistency between model atmosphere structure and abundances used for calculation of synthetic line profiles and interpretation of observed data.

4. Results

4.1. Construction of model atmosphere

In the present analysis we started from chemically homogeneous model atmosphere with the parameters $T_{eff} = 7250$ K and $\log g = 4.3$ and the abundances taken from Ryabchikova et al. (1997) (Model 1). These mean abundances were derived based on the observations close to magnetic maximum, and they provide a satisfactory fit for HARPS observations. Table 2 shows abundances of the elements which were not passed through the subsequent stratification analysis. For the rest of chemical elements the solar composition (Asplund et al. 2005) was assumed.

Based on this model the stratification of Fe, Ba, Ca, Sr, Cr, Si, Pr, and Nd was derived and is displayed on the top panel of

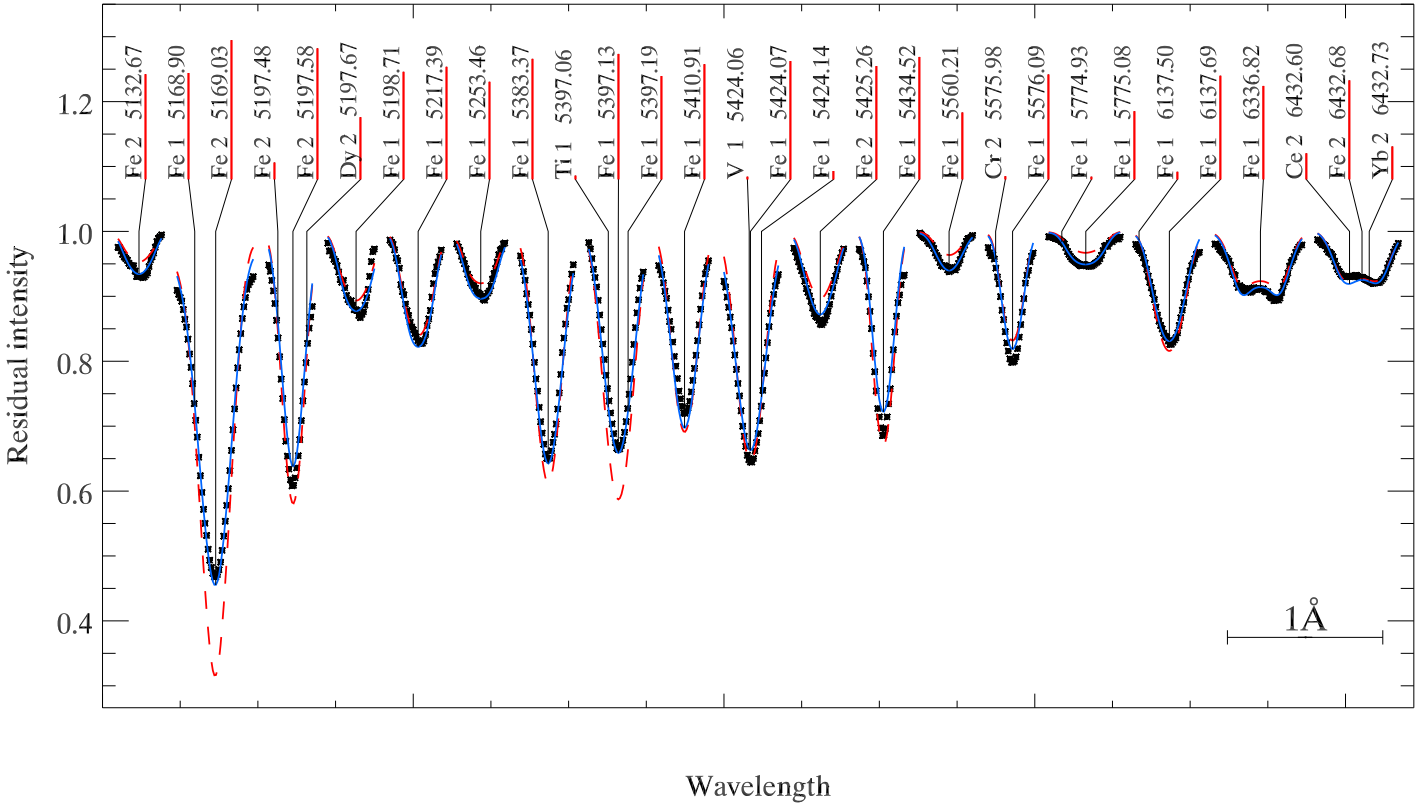


Fig. 2. A comparison between the observed Fe line profiles and calculations with the stratified abundance distribution (full line) and with the homogeneous ($\log(Fe/N_{\text{total}}) = -5.10$) abundances (dashed line).

Fig. 3. It is seen that the stratification of majority of elements shows element underabundance in surface layers and overabundance in layers around star's photosphere ($\log \tau_{5000} \approx [-1, 0]$). Contrary, the distribution of Pr and Nd show inverse picture with the strong overabundance (up to 5 dex) in surface layers. This kind of elements distribution, i.e. the difference between distribution of REE's comparing to other elements, seems to be a common characteristic of the atmospheres of Ap stars (Ryabchikova et al. 2002).

The stratification shown in Fig. 3 (top panel) was then applied to the calculation of new model atmosphere. Again, the individual values of abundances of some other elements used for calculation were taken from Table 2.

The stratification of REE elements and its implementation in model atmosphere computation deserve more detailed description. Numerical calculations showed that the REE elements stratification has a strong influence of model atmosphere structure leading to the appearance of inverse temperature gradient in upper atmospheric region. This is illustrated in Fig. 4, where the models with the same atmospheric parameters and input line list were computed with and without stratification of chemical elements (solid and dotted lines respectively). It is seen that the heating of the stratified atmosphere starts at $\log \tau_{5000} = -3$ going outwards to the stellar surface and reaches its maximal of about 800 K around $\log \tau_{5000} = -4$ compared to homogeneous abundance model. This temperature increase is caused by the presence of REE stratification and, as it seen from Fig. 3, is directly related to the position of abundance jumps of Pr and Nd. No other elements considered in our computations are responsible for such an effect. Indeed, the strong overabundance of Pr and Nd by 4–5 dex relative to their solar values and their rich spectra presented in current version of VALD database make the absorp-

Table 2. Abundances of individual elements.

Element	$\log(N_{\text{el}}/N_{\text{total}})$	$\log(N_{\text{el}}/N_{\text{total}})_{\odot}$
C	-4.00	-3.65
N	-4.50	-4.26
O	-4.00	-3.38
Mg	-5.60	-4.51
Al	-5.57	-5.67
Ti	-7.28	-7.14
Mn	-7.01	-6.65
Co	-5.57	-7.12
Ni	-6.54	-5.81
Y	-7.80	-9.83
La	-9.00	-10.91
Ce	-8.90	-10.46
Sm	-9.00	-11.03
Eu	-9.30	-11.52
Gd	-8.70	-10.92
Dy	-8.94	-10.90
Er	-9.53	-11.11

The abundances derived from observations are from Ryabchikova et al. (1997). The REE's abundances were derived using the lines of the first ions. The solar abundances are taken from Asplund et al. (2005).

tion coefficient to be very high at frequencies of REE transitions. The latter are generally located at the spectral region where the star with $T_{\text{eff}} = 7250$ K radiates most of its energy dominating in the total radiative energy balance, and thus allowing for the heating of atmospheric layers with high REE opacity.

The appearance of inverse temperature gradient clearly shows that the REE elements are no longer trace elements in atmospheres of Ap stars if their stratification is as strong (or com-

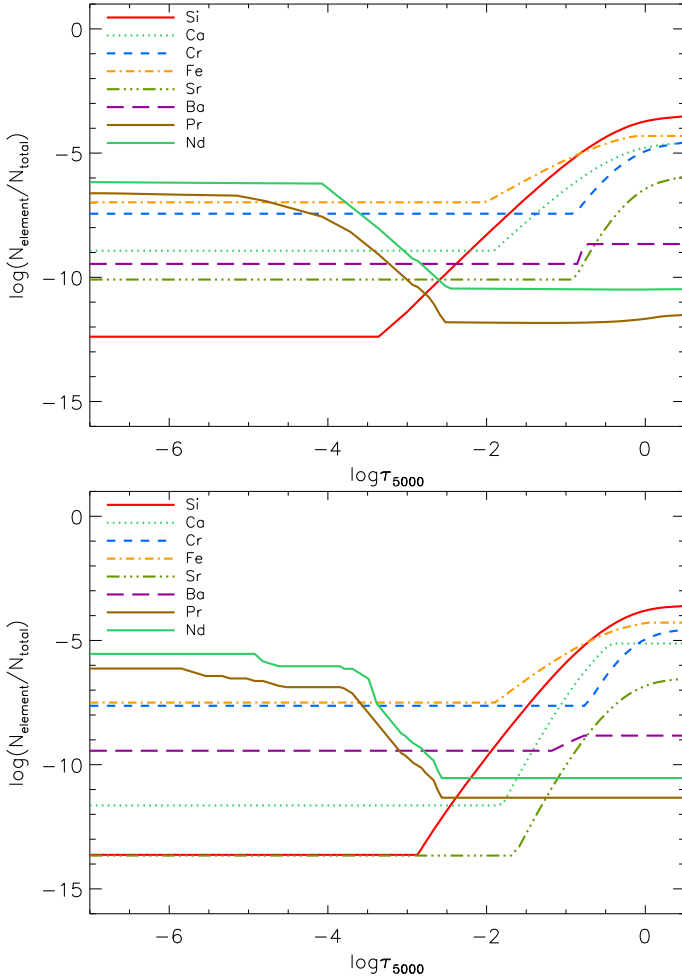


Fig. 3. Stratification of eight elements in atmosphere of HD 24712 derived using homogeneous first-approximation model (Model 1, top panel) and using final model with scaled REE opacity (Model 5, bottom panel).

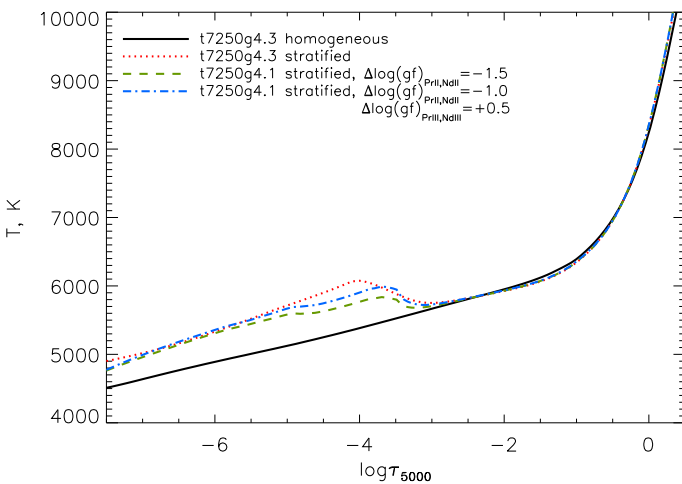


Fig. 4. Effect of Pr and Nd stratification on model temperature structure. Solid line – t7250g4.3 model calculated with homogeneous abundances; dotted line – t7250g4.3 model calculated with stratified abundances shown in Fig. 3; dashed and dash-dotted lines – t7250g4.1 models calculated with stratified abundances and scaled Pr II, III and Nd II, III $\log(gf)$ values.

parably strong) as in the atmosphere of HD 24712. This immediately implies that not only synthetic line profiles, but also model atmospheres with REE stratification must be computed based on NLTE line formation for REE's. Unfortunately, this can not be done with the current version of LLMODELS. Nevertheless, to simulate NLTE effects of Pr and Nd in model atmosphere calculations we used the following approach. Mashonkina et al. (2005) and Mashonkina et al. (2009) found that, for the stratified distribution of Nd and Pr, the NLTE abundance corrections are positive for the lines of the first ions at a level of one order of magnitude and negative for the lines of the second ions at a level of ≈ 0.5 dex. Thus, to account for the REE stratification in LTE model atmosphere code, we scale the $\log(gf)$ values of Pr II and Nd II lines by -1.5 dex while taking abundances derived using second ions for model atmosphere calculation. This procedure was applied to all the Pr II and Nd II lines that are presented in master line list used for model atmosphere calculations. Then, using this new line list, we recomputed the model atmosphere and re-derived stratification of chemical elements again. At each iteration Pr and Nd stratifications were recalculated based on NLTE line formation for Pr II/III and Nd II/III. The best fit to hydrogen H α line profile (wings) and photometric color-indices required the decrease of effective gravity down to $\log g = 4.1$ (mainly to fit c_1 index). No further noticeable changes were detected in observed parameters and this gravity was considered as a final one. The model and stratification calculations are converged after the second iteration (Model 4).

Except Pr and Nd, other REE elements can also be non-uniformly distributed in the atmosphere of HD 24712 and can also exhibit deviations from LTE. Among them, only most abundant elements may play a noticeable role in modification of atmospheric structure. At present, we do know neither distributions of these elements, nor the magnitude of their NLTE effects. In any case, preliminary abundance results for Ce and Sm show that REE anomaly – a discrepancy between abundances inferred from the lines of singly- and doubly-ionized element – reaches approximately the same magnitude as for Pr and Nd. Supposing that the Ce (which has the biggest number of available lines in VALD among other REE elements) has the same vertical distribution as Nd, we estimated its effect on atmospheric structure. We found that neglecting Ce stratification we underestimate a size of temperature jump by no more than ~ 200 K.

Decreasing the $\log(gf)$ values of Pr II and Nd II lines could, in principle, simulate the NLTE line opacity of these elements, however the second ions are also affected by NLTE effects that bring as much as 0.5 dex difference between LTE and NLTE abundances derived using second ions spectra. This forced us to compute another model where the $\log(gf)$ values of both first and second ions are changed by -1 dex and 0.5 dex respectively (Model 5). This model provides slightly higher temperature increase in superficial layers compared with the model where $\log(gf)$ values of only first ions were changed (see Fig. 4). It is seen that the simulation of NLTE REE opacity tends to decrease the amplitude of the temperature jump almost by a factor of two. However, independently on the way how to scale the REE opacity, the overall picture remains the same illustrating the heating of surface layers in the region of strong Pr and Nd overabundance.

We also tested the influence of Pr II and Nd II bound-free opacity on model structure and energy distribution. To simplify the computations we assumed three characteristic energy levels with excitation energies of 2 eV, 3 eV, and 4 eV for both ions. These levels further consist of 50 atomic states each with the statistical weight $g = 7$. Such an approximation is based on the fact

Table 3. Observed and calculated photometric parameters of HD 24712.

Color index	Observations	t7250g4.3 homogeneous	t7250g4.3 stratified REE unscaled	t7250g4.1 stratified REE unscaled	t7250g4.1 stratified $\Delta \log(gf)_{\text{PrII,NdII}} = -1.5$	t7250g4.1 stratified $\Delta \log(gf)_{\text{PrII,NdII}} = -1$
		(Model 1)	(Model 2)	(Model 3)	(Model 4)	$\Delta \log(gf)_{\text{PrII,NdIII}} = +0.5$ (Model 5)
<i>b-y</i>	0.186 (0.003); 0.191*	0.195	0.188	0.183	0.180	0.180
<i>m₁</i>	0.202 (0.006); 0.211*	0.197	0.214	0.213	0.205	0.207
<i>c₁</i>	0.653 (0.011); 0.626*	0.610	0.575	0.638	0.663	0.656
<i>Hβ</i>	2.745 (0.003); 2.760*	2.802	2.804	2.808	2.810	2.809
<i>a</i>	0.609 (0.0005)	0.621	0.621	0.621	0.617	0.619
<i>B-V</i>	0.320	0.308	0.308	0.297	0.288	0.290
<i>U-B</i>	1.381	1.333	1.311	1.370	1.379	1.376
<i>V-B</i>	0.572	0.596	0.595	0.610	0.621	0.619
<i>B₁-B</i>	0.978	0.984	0.990	0.985	0.982	0.983
<i>B₂-B</i>	1.393	1.413	1.407	1.413	1.417	1.416
<i>V₁-B</i>	1.286	1.319	1.319	1.333	1.343	1.341
<i>G-B</i>	1.688	1.727	1.726	1.741	1.753	1.751

* – Martinez (1993)

The values in brackets give the error bars of observations.

that both ions have essentially the same structure of states with the very close ionization potentials. The NLTE level populations were taken directly from DETAIL code and then incorporated in LLMODELS. For all the levels, the photoionization cross-sections were calculated using the hydrogenic approximation. It appeared that the effect of the Pr II and Nd II bound-free opacity becomes visible only if the abundances of these elements are increased by +6 dex for the stratified model where REE's are already in strong overabundance in surface layers. Even so, the cumulative effect on the temperature distribution was never higher than tens of K. We, thus, concluded that REE bound-free opacity can be ignored in the model atmosphere computations.

Bottom panel of Fig. 3 shows the stratification derived with Model 5. One can note that the stratification of REE's shows more steep abundance jump in this case which is probably a result of more refined set of optical depths around REE jump implemented in the last iteration compared to the initial model and the first iteration. This is also the reason why the inverse temperature gradient shown in Fig. 4 is more steep for the model calculated with Model 5 stratification than for the model with stratification derived in Model 4. Few remarks concerning Sr and Ba stratification calculations should be made. Although we get formally Ba stratification, it is not significant because the difference between χ^2 for line profiles fits with uniform and stratified models does not exceed 15-16%, while χ^2 differs by 5-10 times in the case of real stratification. Therefore uniform Ba distribution in the atmosphere of HD 24712 or at least in the layers where the studied Ba II lines are formed is more probable. For Sr distribution we used five lines with three weakest lines of Sr I. Strontium distribution is mainly based on strong Sr II lines, in particular, on resonance Sr II λ 4215.5 Å. The wings of Sr II lines that probe abundance in the deeper atmospheric layers, are blended, that obviously leads to larger formal computing errors of stratification parameters determination and, hence, to worse χ^2 . To check a reliability of Sr stratification we recalculated it using Sr lines observed at slightly different magnetic phase 0.944 (see UVES time-series observations in Ryabchikova et al. (2007)). Within the formal errors of DDAFIT procedure strontium abundance profiles coincide below $\log \tau_{5000} = -2$ where practically all considered Sr lines are formed. They differ above $\log \tau_{5000} = -2$, where the only core of Sr II λ 4215.5 Å line is formed. Poor fit of

this line in the transition region between the line core and the line wings indicates that a more complex shape of abundance profile than a simple step-function is required to describe the observed line profile, similar to the Ap star HD 133792 (Kochukhov et al. 2006). Strontium stratification derived for HD 24712 is not spurious, but the shape of the Sr abundance profile may differ from that derived in the present study. The other elements that demonstrated strong changes during iterative stratification analysis are Si and Ca. Both elements show the increase of the abundance jump amplitude in the final stratification with strong underabundance in surface layers and with practically the same abundance near photospheric layers. The jump itself becomes steeper. It may be caused by the change in temperature and electron density structure of the atmosphere above $\log \tau_{5000} = -3$, where the central parts of the strongest Ca I λ 4227 and Si II $\lambda\lambda$ 6347,6371 are formed. However, the formal errors of Si and Ca abundances in the upper atmospheric layers derived in DDAFIT procedure are rather high, up to 1.5 dex, hence 2.5 dex difference for the initial and final Ca distributions may be considered as within the 3σ limit.

The changes in element distributions between the two cases shown in Figs. 3 are purely due to the changes in model atmosphere structure. Thus we can conclude that the recalculation of the model atmosphere structure could be very important for the quantitative stratification analysis. For some elements, the stratification derived with models computed under the assumption of homogeneous elements distribution can be considered only as a first approximation.

Finally, in Table 3 we compare theoretical and observed photometric color-indices of HD 24712. The calculations are presented for two models with $T_{\text{eff}} = 7250$ K, $\log g = 4.3$ (homogeneous and stratified abundances) and for three models with $T_{\text{eff}} = 7250$ K, $\log g = 4.1$ but with different assumptions about Pr and Nd opacity. The theoretical colors were calculated with modified computer codes taken from Kurucz (1993a). One can see that the color-indices of Strömgren system as well as *U* – *B* and *V* – *B* indices of Geneva system are better represented by stratified models. In contrast, the last two Geneva indices given in Table 3 are better described by homogeneous abundance model. However, these differences are not very big and we can conclude that, generally, the two final models cal-

culated with the complex stratification shown in Fig. 3 (bottom panel) and scaled REE opacity demonstrates a good agreement with the observations. We have to note that the Strömgren photometry taken from Martinez (1993), which is not available in electronic format, introduces additional uncertainties. In particular, index $b - y$ of Martinez (1993) is better represented by homogeneous model. Furthermore, the difference of 0.027 mag between the two observations for c_1 index (see Table 3) does not allow to distinguish definitely between homogeneous and stratified models. On the other hand, the observation of c_1 taken from Hauck & Mermilliod (1998) agrees nicely with predictions by model with scaled Pr II,III and Nd II,III opacity. The difference of 0.007 mag between models computed under two assumptions about the scaling of REE opacity (last two models in Table 3) is within the error bars of observations, but deviates significantly from c_1 calculated without REE scaling. Our calculations demonstrate that taken stratification effects into account we obtain lower surface gravity than follows from the calibrations based on homogeneous models. Strong impact of simulated NLTE effects of Pr and Nd on c_1 value, temperature distribution, and colors demonstrates a necessity of more precise model atmosphere computations with accurate treatment of Pr, Nd, and possibly other REE lines formation. Our choice of $\log g$ for the final model could also change as more advanced NLTE model atmospheres are employed. Moreover, the strong variability in c_1 index with the peak-to-peak amplitude of 0.086 mag (Wolff & Morrison 1973) is likely to be responsible for the difference between the value of Martinez (1993) and the average value given by Hauck & Mermilliod (1998). Thus, at present it is difficult to say something more definite about the $\log g$ value of the star and we restrict ourselves with $\log g = 4.1$.

As it was stated above, for the opacity calculation in model atmospheres we used REE data extracted from VALD database. However, for the NLTE calculations with DETAIL code it was necessary to have more extensive line lists for accurate calculations of radiative rates for every single atomic state. These detailed line lists for Pr II and Nd II,III were produced in Institute of Spectroscopy (ISAN, Russia), and described in Mashonkina et al. (2005, 2009). Note that the ISAN data already contains Pr and Nd parameters from VALD thus providing only additional number of predicted lines. For example, while VALD provides information about 508 Pr II , 1279 Nd II , and 55 Nd III lines, ISAN theoretical computations extended them up to 103428, 1172579, and 6858 lines respectively. However, this great increase in line numbers showed only marginal changes in model temperature distribution. This allowed to conclude that the radiative equilibrium balance in atmosphere of HD 24712 is controlled by strongest REE lines that are presented in VALD. The only noticeable changes were detected for the c_1 (increased by 0.012 mag) and for m_1 index (decreased by 0.008 mag).

Fig. 6 demonstrates the observed and predicted energy distributions of HD 24712. Observational data is represented by a combination of the IUE low-resolution flux and photometric measurements converted to absolute flux units. The theoretical fluxes are calculated with the last model from Table 3. Note that all the models from Table 3 represent observations good enough, and the only possibility to choose the best one would be the comparison of UV fluxes blueward $\lambda = 2000\text{\AA}$ where stratified models predict significant flux excess (almost one order of magnitude in maximum) compared to homogeneous abundance model, but this region plays unimportant role in the total energy balance in the atmosphere due to the relatively cool effective temperature of the star. Although the IUE observations tend to be closer to the theoretical stratified fluxes at this region, it is difficult to make

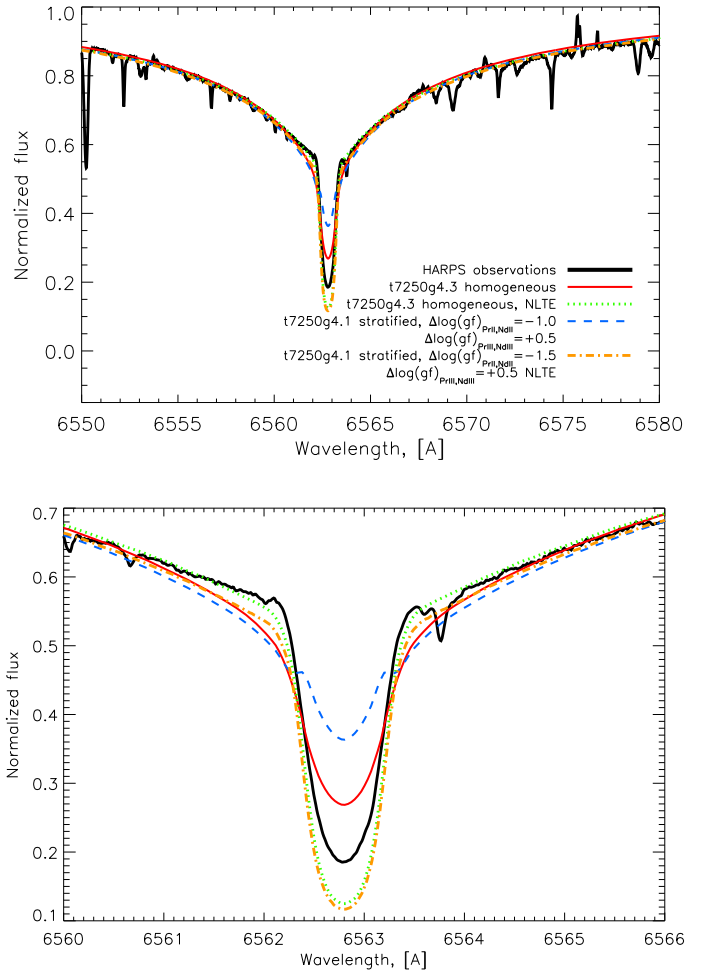


Fig. 5. Observed and calculated H α line profiles. Thick full line – HARPS observations; dotted line – model with $T_{\text{eff}} = 7250\text{ K}$, $\log g = 4.3$ and with homogeneous elements distribution; full line – model with $T_{\text{eff}} = 7250\text{ K}$, $\log g = 4.3$ and with stratification shown in 3 (top panel); dashed line – model with $T_{\text{eff}} = 7250\text{ K}$, $\log g = 4.1$ and with final iteration shown in 3 (bottom panel). Bottom panel shows the zoomed part of the figure on top panel around the core of the line.

a clear decision because of large error bars in observations (see IUE data archive).

Fitting of the spectral energy distribution of HD 24712 calibrated in physical flux units allows us to derive the angular diameter of the star, $\theta = 0.335 \pm 0.005$ mas. Combined with the revised Hipparcos parallax of $\pi = 20.32 \pm 0.39$ mas (van Leeuwen 2007), this yields a new determination of the stellar radius, $R = 1.772 \pm 0.043 R_{\odot}$.

4.2. Effect of REE stratification

It was shown above that the accumulation of Pr and Nd leads to the appearance of inverse temperature gradient with the temperature jump of about 600 K as compared to non-stratified model. However, this temperature jump is located in upper atmospheric layers and has no influence on the wings of H α line, as it is shown in Fig. 5. Thus, even in the case of strong stratification of REE elements, the determination of atmospheric stellar parameters by fitting the wings of hydrogen lines could be performed with the model not taking the stratification of REE into account.

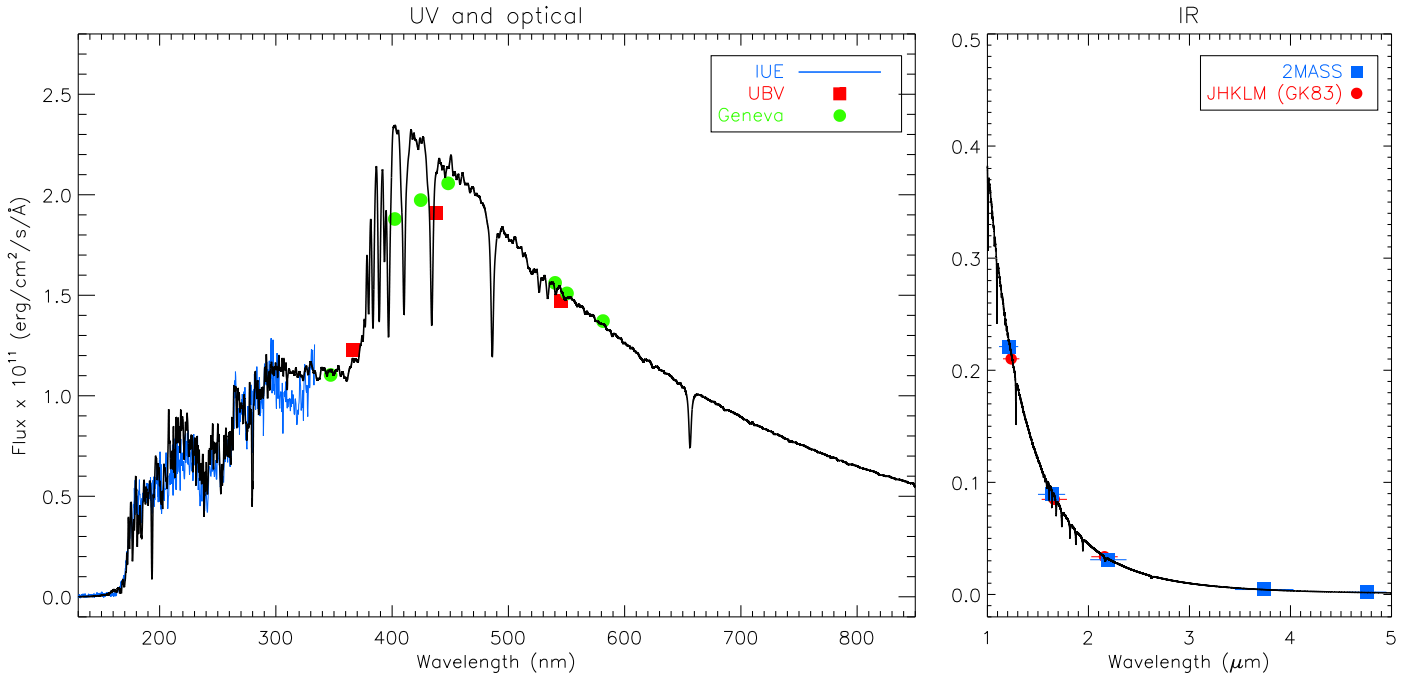


Fig. 6. Calculated and observed energy distributions of HD 24712. Solid line – t7250g4.1 model calculated with stratified abundances shown in Fig. 3 (bottom panel) and changed $\text{Pr}_{\text{II,III}}$ and $\text{Nd}_{\text{II,III}}$ $\log(gf)$ values by -1 dex and $+0.5$ dex respectively.

However, LTE calculations show that the core of $\text{H}\alpha$ line is influenced strongly by stratification of Pr and Nd (bottom panel of Fig. 5). One could see that none of the $\text{H}\alpha$ profiles computed under the assumption of LTE line formation could fit the transition region between the line core and wing, that is commonly called as core-to-wing anomaly (CWA) and is frequently observed in spectra of Ap stars. Kochukhov et al. (2002) tried to explain this anomaly by the existence of the temperature bump in the upper atmospheric layers above $\log \tau_{5000} \approx -1$. What is interesting is that the heating of atmospheric layers due to REE stratification produces the same sharp transition between the line wings and core, but the central intensity of theoretical spectra are much shallower than that with homogeneous abundance model which still provides the best fit. However, all stratification effects disappear when NLTE hydrogen lines formation is applied, which is ‘washing out’ all stratification effects.

From Figs. 2 and 3 of Kochukhov et al. (2002) it is seen that in order to explain the core-to-wing anomaly of hydrogen Balmer lines, the temperature jump should be located between $\log \tau_{5000} \approx -3$ and -2 . In our calculations the temperature gradient starts higher in stellar atmosphere at $\log \tau_{5000} \approx -3$. Position of the temperature gradient caused by REE stratification depends on the details of NLTE line formation, but it is practically impossible to shift REE jump position in HD 24712 downward by more than $0.3 - 0.5$ dex in $\log \tau_{5000}$ scale (Mashonkina et al. 2009).

REE stratification is not the only reason for inverse temperature gradients in Ap star atmosphere. Recently, Alecian & Stift (2007) and LeBlanc et al. (2009) calculated element stratification in the atmospheres with magnetic field and showed that horizontal magnetic field changes abundance distribution. Instead of a step-like shape which is obtained in diffusion calculations in non-magnetic atmospheres or in the presence of predominantly vertical component of the field, one gets an abundance minimum and then an increase of element abundance in the up-

permost atmospheric layers. These abundance increase might lead to the corresponding temperature increase started just at $\log \tau_{5000} = -1$ (see Fig. 5 of LeBlanc et al. 2009). In a simple step function approximation used in the present stratification analysis as well as in the most other similar studies (Wade et al. 2001; Ryabchikova et al. 2005, 2006, 2008), we cannot probe an increase of element abundance in the uppermost atmospheric layers. However, relatively good fitting of the observed line profiles in many stars with different strengths of magnetic field obtained with step-like abundance distribution of Si, Ca, Cr, Fe – main contributors to line opacities – supports the absence of significant increase of element abundance immediately following the abundance jump. This is further corroborated by the vertical inverse problem solution for the Ap star HD 133792 (Kochukhov et al. 2006), where the authors were able to derive element distribution without *a priori* assumption about the shape of this distribution. One should note, however, that this method can be currently applied only to non-magnetic or weakly magnetic atmospheres. Additionally, in atmospheric diffusion calculations the stratification is generally obtained assuming that all the forces acting on a given plasma volume are in stationary equilibrium (total diffusion velocity is zero). Regarding to real stars this is not necessarily the case and element stratifications at a given moment could be different (see Alecian & Stift 2007).

Thus, to explain the most part of the observed peculiarities in cool Ap stars we need to implement the full NLTE treatment of REE elements in model atmosphere calculations and not the rough simulation presented in this study. The accumulation of other elements could also be responsible for CWA and more detailed investigation is needed to explore this effect.

5. Conclusions

The spectroscopic investigation of elements stratification is the only method for testing modern predictions of the particle diffusion theory in atmospheres of star where this mechanism is

sufficient to produce detectable abundance gradients. It provides us with stratification profiles of different chemical elements that could be compared with recent self-consistent diffusion models. However, in most of the stratification analysis routines the standard stellar model atmospheres are used where the homogeneous abundances are assumed.

To circumvent this difficulty we made an attempt to construct an empirical self-consistent model atmosphere where the stratification of chemical elements is derived directly from observed spectra and then treated in a model atmosphere code. This iterative procedure was applied to one of the cool CP star HD 24712. Below we summarise the main results of this investigation:

- The accumulation of Pr and Nd in the upper atmosphere has an impact on the temperature structure of the atmosphere. The strong overabundance of these elements leads to an appearance of inverse temperature gradient with the maximum temperature increase of up to 600 – 800 K as compared to homogeneous abundance model.
- For HD 24712 we find that the effect of elements stratification has minor influence on the observed energy distribution. The lack of good quality observations in UV region (where the effect of stratification is more pronounced) does not allow at present to carry out more precise investigations. The changes in temperature structure due to the stratification of Pr and Nd do not affect the wings of hydrogen lines and thus can be ignored in routine procedures of the determination of atmospheric stellar parameters.
- Due to their high overabundance and important role in overall temperature balance, REE element can no longer be considered as trace elements in standard scheme of NLTE calculations. This implies that, to achieve a better consistency in modelling of REE stratification, the model atmosphere should account for REE NLTE effects as well.
- For HD 24712 we find no critical changes in the shape and amplitude of stratification profiles of chemical elements when recalculating the atmospheric temperature-pressure structure. Most of the changes are comparable with the error bars of the minimization procedure used.

Acknowledgements. This work was supported by following funding projects: FWF Lisa Meitner grant Nr. M998-N16 (DS), FWF P17890-N2 (TR), RFBR 08-02-00469-a and Presidium RAS Programme “Origin and evolution of stars and galaxies” (TR and LM). We also acknowledge the use of electronic databases (VALD, SIMBAD, NASA’s ADS).

References

- Achmad, I., de Jager, C., & Nieuwenhuijzen, H. 1991, A&A, 250, 445
- Alecian, G., Stift, M. J. 2007, A&A, 475, 659
- Asplund, M., Grevesse, N., & Sauval, A. J. 2005, in ASP Conf. Ser. 336, Cosmic Abundances as Records of Stellar Evolution and Nucleosynthesis, ed. Thomas G. Barnes III & Frank N. Bash, 25
- Babel, J. 1992, A&A, 258, 449
- Bard, A., & Kock, M. 1994, A&A, 282, 1014
- Bard, A., Kock, A., & Kock, M. 1991, A&A, 248, 315
- Black, J.H., Wisheit, J.C., & Laviana, E. 1972, ApJ, 177, 567
- Blackwell, D.E., Petford, A.D., & Shallis, M.J. 1979, MNRAS, 186, 657
- Blackwell, D.E., Petford, A.D., & Shallis, M.J. 1982, MNRAS, 210, 595
- Blanco, F., Botho, B., & Campos, J. 1995, Phys. Scr., 52, 628
- Burki, G., Grenon, M., Richard, C., Pernier, B., Nicolet, B., & Cramer, N. 1999, Geneva Photometric Database, <http://obswww.unige.ch>
- Butler, K., & Giddings, J. 1985, Newsletter on the analysis of astronomical spectra No. 9, University of London
- Fleurier, C., Sahal-Brechet, S., & Chapelle, J. 1977, JQSRT, 17, 595
- Garcia, G., & Campos, J. 1988, J. Quant. Spec. Radiat. Transf., 39, 477
- Garz, T. 1973, A&A, 26, 471.
- Goncharsky, A. V., Stepanov, V. V., Khokhlova, V. L., & Yagola, A. G. 1982, Astron. Zh., 59, 1146
- Hauck, B., Mermilliod, M. 1998, A&AS, 129, 431
- Hauschildt, P., Allard, F., Baron, E. 1999, ApJ, 512, 377
- Hui-Bon-Hoa, A., LeBlanc, F., Hauschildt, P. H. 2000, ApJ, 535, L43
- Khan, S., & Shulyak, D. 2007, A&A, 469, 1083
- Khan, S., & Shulyak, D. 2006, A&A, 448, 1153
- Khokhlova, V.L., Vasilchenko D.V., Stepanov, V.V., & Romanyuk, I.I. 2000, AstL, 26, 177
- Kochukhov, O. 2007, in *Physics of Magnetic Stars*, eds. D.O. Kudryavtsev and I.I. Romanyuk, Nizhniy Arkhyz., p.109
- Kochukhov, O., Tsymbal, V., Ryabchikova, T., Makaganyk, V., & Bagnulo, S. 2006, A&A, 460, 831
- Kochukhov, O., Khan, S., & Shulyak, D. 2005, A&A, 433, 671
- Kochukhov, O., Bagnulo, S., Wade, G. A. et al. 2004a, A&A, 414, 613
- Kochukhov, O., Drake, N. A., Piskunov, N., de la Reza, R. 2004b, A&A, 424, 935
- Kochukhov, O., Bagnulo, S., Barklem, P. S. 2002, ApJ, 578, L75
- Kupka, F., Piskunov, N., Ryabchikova, T. A., Stempels, H. C., & Weiss, W. W. 1999, A&AS, 138, 119
- Kurucz, R. L. 1993, Kurucz CD-ROM 13, Cambridge, SAO
- LeBlanc, F., Monin, D., Hui-Bon-Hoa, A., & Hauschildt, P.H. 2009, A&A, in press
- Lueftinger, T., Kuschnig, R., Piskunov, N. E., Weiss, W. W. 2003, A&A, 406, 1033
- Martin, G.A., Fuhr, J.R., & Wiese, W.L. 1988, J. Phys. Chem. Ref. Data, 17, Suppl.3
- Martinez, P. 1993, Ph.D. Thesis, University of Cape Town, SA
- Mashonkina, L. I., Korn, A.J., Przybilla, N. 2007, A&A, 461, 261
- Mashonkina, L., Ryabchikova, T., Ryabtsev, A. 2005, A&A, 441, 309
- Mashonkina, L., Ryabchikova, T., Ryabtsev, A., Kildiyarov, R. 2009, A&A, 495, 297
- Mashonkina, L., Zhao, G., Gehren, T. et al. 2008, A&A, 478, 529
- Michaud, G. 1970, ApJ, 160, 641
- Miles, B.M., & Wiese, W.L. 1969, NBS Technical Note 474.
- Nilsson H., Ljung G., Lundberg H., & Nielsen K.E. 2006, A&A, 445, 1165
- Piskunov, N.E., Wehlau, W.H. 1990, A&A, 233, 497
- Piskunov, N. E., Kupka, F., Ryabchikova, T. A., Weiss, W. W., & Jeffery, C. S. 1995, A&AS, 112, 525
- Piskunov, N. E. 1999, in 2nd International Workshop on Solar Polarization, eds. K. Nagendra and J. Stenflo, Kluwer Acad. Publ. ASSL, 243, 515
- Raassen, A.J.J., & Uylings, P.H.M. 1998, A&A, 340, 300
- Ryabchikova, T., Kochukhov, O., & Bagnulo S. 2008, A&A, 480, 811
- Ryabchikova, T., Sachkov, M., Weiss, W.W., et al. 2007, A&A, 462, 1103
- Ryabchikova, T., Ryabtsev, A., Kochukhov, O., Bagnulo, S. 2006, A&A, 456, 329
- Ryabchikova, T., Leone, F., Kochukhov, O. 2005, A&A, 438, 973
- Ryabchikova, T., Piskunov, N., Kochukhov, O. et al. 2002, A&A, 384, 545
- Ryabchikova, T., Wade, G., & LeBlanc, F. 2003, in IAU Symposium No. 210, Modelling of Stellar Atmospheres, eds. N.E. Piskunov, W.W. Weiss, & D.F. Gray, ASP, 301
- Ryabchikova, T.A., Landstreet J.D., Gelbmann M.J., et al. 1997, A&A, 327, 1137
- Rybicki, G.B. & Hummer, D.G. 1991, A&A, 245, 171
- Rybicki, G.B. & Hummer, D.G. 1992, A&A, 262, 209
- Shulyak, D., Tsymbal, V., Ryabchikova, T., Stütz Ch., & Weiss, W. W. 2004, A&A, 428, 993
- Seaton, M. J., Mihalas, D., & Pradhan, A. K. 1994, MNRAS, 266, 805
- Smith, G. 1988, J. Phys. B, 21, 2827
- Smith, G., & Gallagher, A. 1966, Phys. Rev., 145, 26
- Smith, G., & O’Neil, J. A. 1975, A&A, 38, 1
- Smith, G., & Raggett, D.St.J. 1981, J. Phys. B, 14, 4015
- van Leeuwen, F. 2007, Hipparcos, the New Reduction of the Raw Data. Astrophysics and Space Science Library, Springer
- Vogt, N., Kerschbaum, F., Maitzen, H.M., & Faundez-Abans, M. 1998, A&AS, 130, 455
- Wade, G.A., Ryabchikova, T.A., Bagnulo, S., & Piskunov, N. 2001, in Magnetic Fields across the Hertzsprung-Russel Diagram, ed. G. Mathys, S.K. Solanki & D.T. Wickramasinghe, ASP Conf. Ser., 248, 373
- Warner, B. 1968, MNRAS, 139, 115
- Wolff, Sidney C., Morrison, Nancy D. 1973, PASP, 85, 141

Online Material

List of Objects

'HD 24712' on page 1

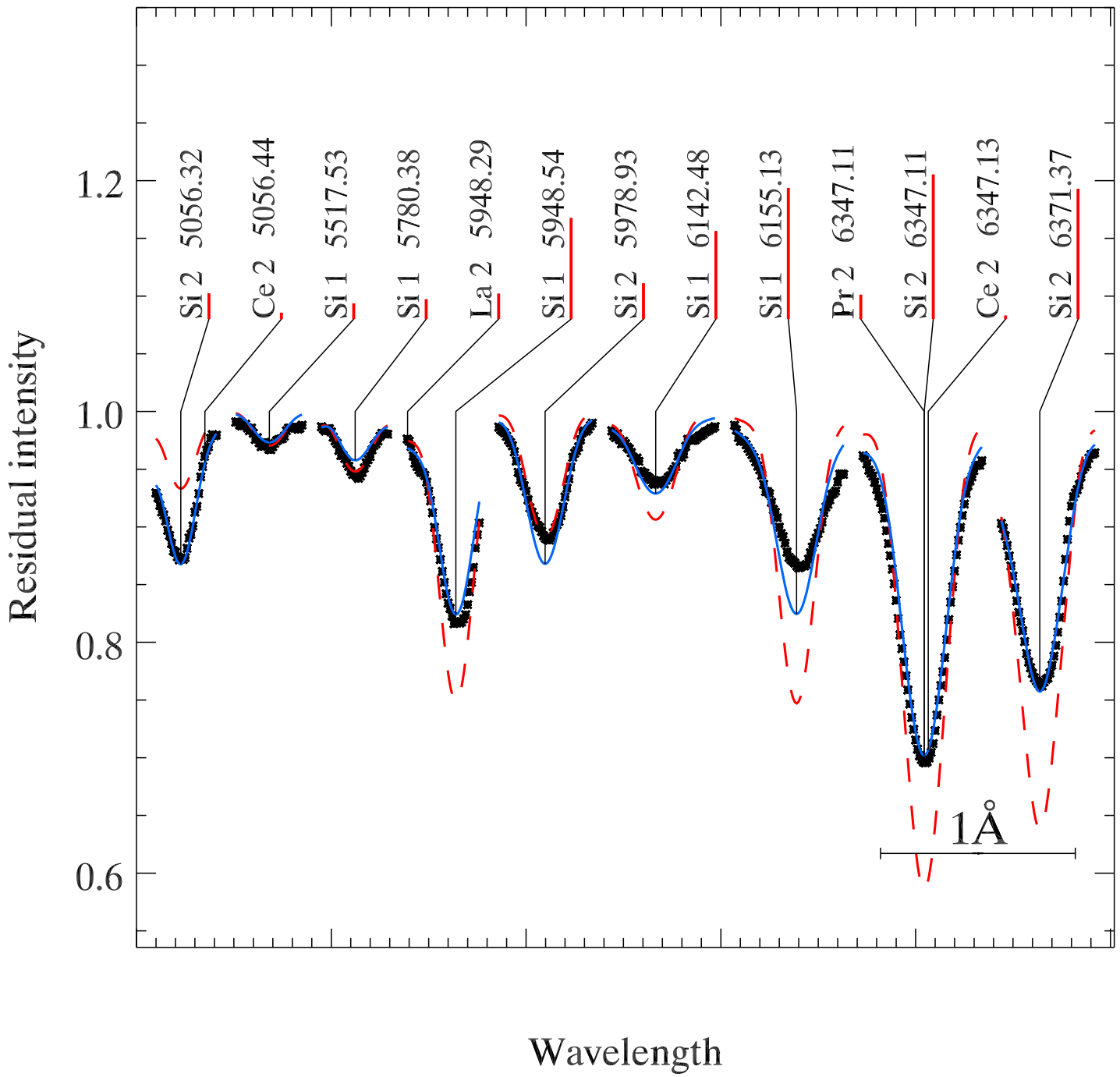


Fig. 7. A comparison between the observed Si line profiles and calculations with the stratified abundance distribution (full line) and with the homogeneous ($\log(S\ i/N_{\text{total}}) = -4.50$) abundances (dashed line).

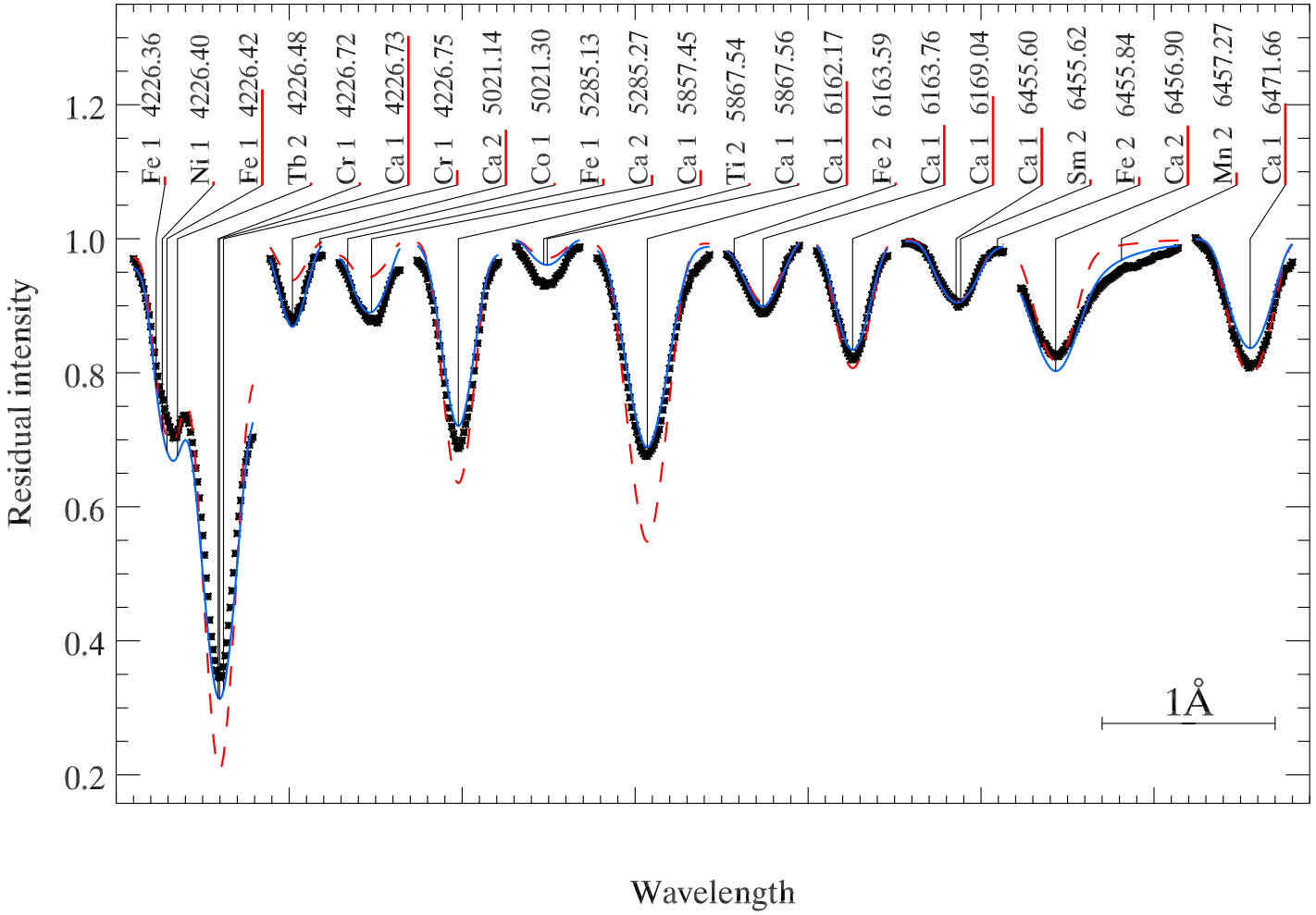


Fig. 8. A comparison between the observed Ca line profiles and calculations with the stratified abundance distribution (full line) and with the homogeneous ($\log(Ca/N_{\text{total}}) = -5.80$) abundances (dashed line).

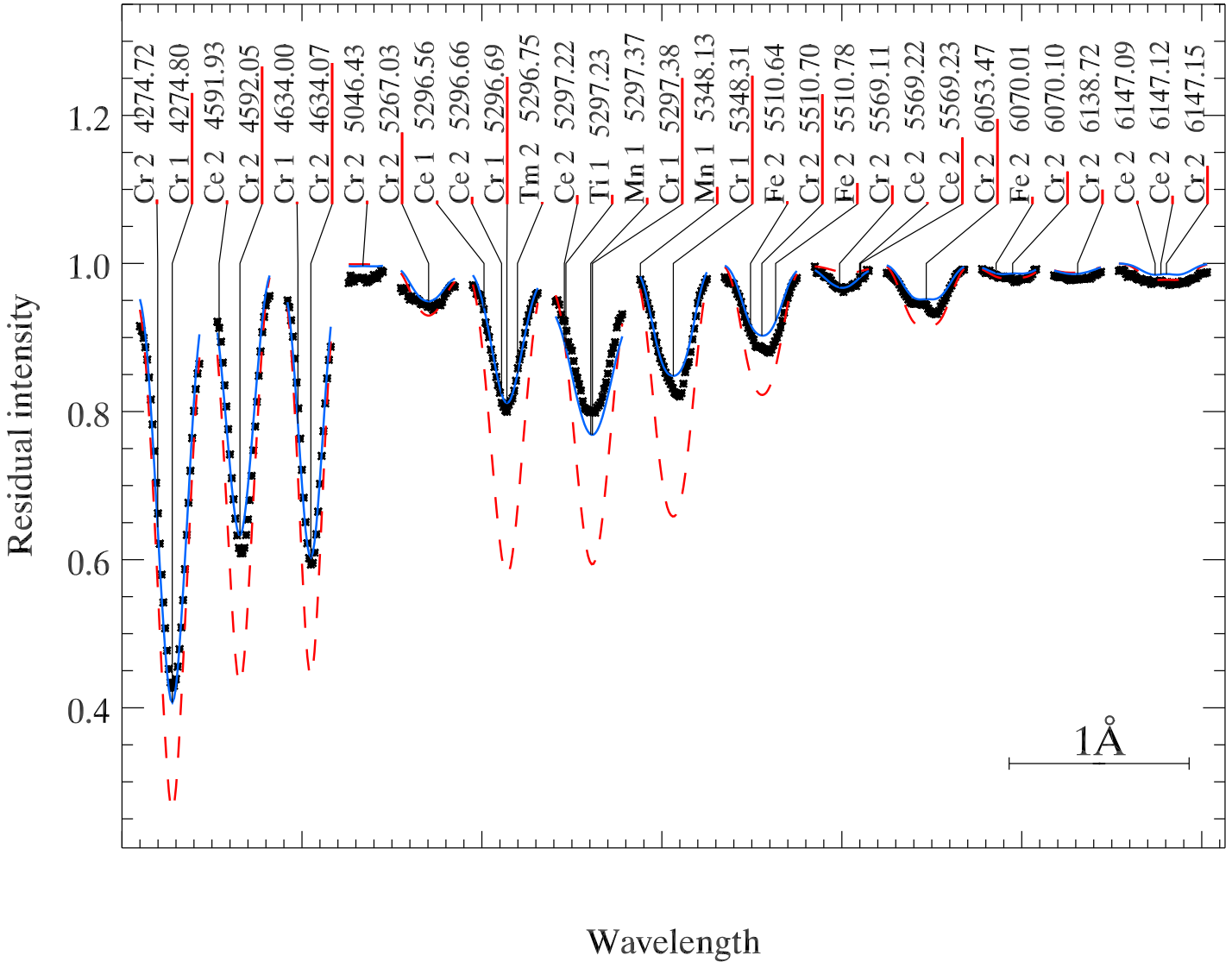


Fig. 9. A comparison between the observed Cr line profiles and calculations with the stratified abundance distribution (full line) and with the homogeneous ($\log(Cr/N_{\text{total}}) = -5.80$) abundances (dashed line).

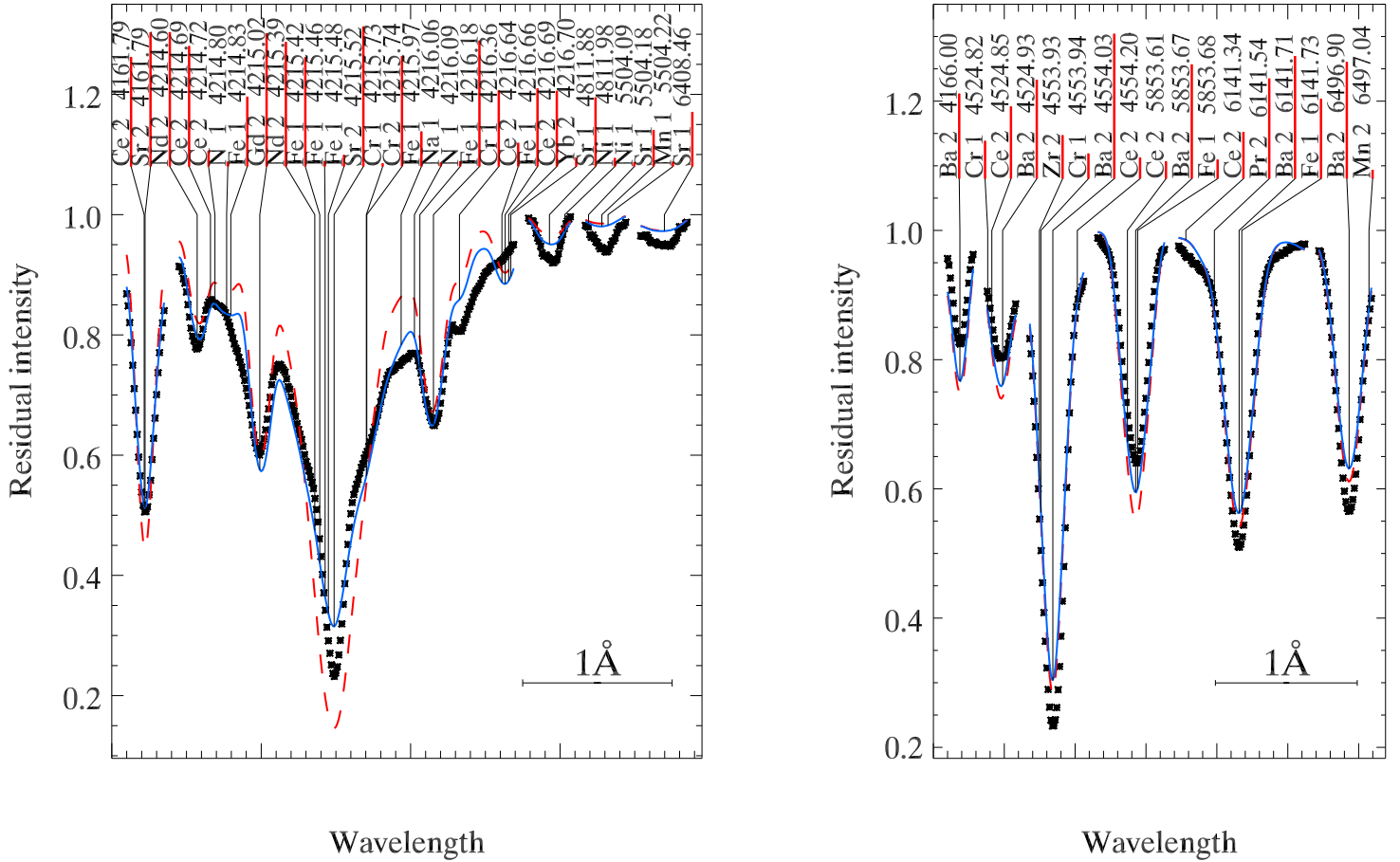


Fig. 10. A comparison between the observed Sr (left panel) and Ba (right panel) line profiles and calculations with the stratified abundance distribution (full line) and with the homogeneous ($\log(Sr/N_{\text{total}}) = -8.00$, $\log(Ba/N_{\text{total}}) = -9.00$) abundances (dashed line).